JOURNAL OF THE AMERICAN CHEMICAL SOCIETY

Article

Role of the Orbitally Degenerate Mn(III) Ions in the Single-Molecule Magnet Behavior of the Cyanide Cluster {[Mn(tmphen)][Mn(CN)]} (tmphen = 3,4,7,8-tetramethyl-1,10-phenanthroline)

Andrei V. Palii, Sergei M. Ostrovsky, Sophia I. Klokishner, Boris S. Tsukerblat,
Curtis P. Berlinguette, Kim R. Dunbar, and Jos Ramn Galn-Mascars

J. Am. Chem. Soc., **2004**, 126 (51), 16860-16867• DOI: 10.1021/ja046771a • Publication Date (Web): 02 December 2004

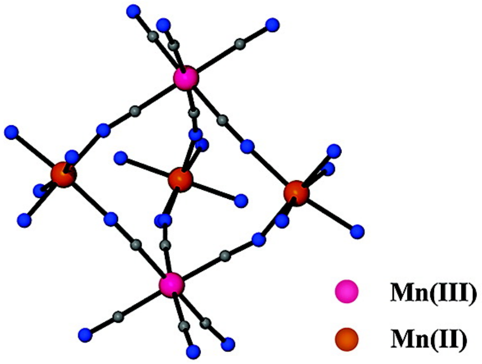

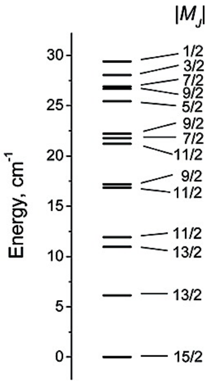

ACS Publications
High quality. High impact.

Journal of the American Chemical Society is published by the American Chemical Society. 1155 Sixteenth Street N.W., Washington, DC 20036

J|A|C|S
ARTICLES

Role of the Orbitally Degenerate Mn(III) Ions in the Single-Molecule Magnet Behavior of the Cyanide Cluster $\{[Mn^{II}(tmphen)_2]_3[Mn^{III}(CN)_6]_2\}$ (tmphen = 3,4,7,8-tetramethyl-1,10-phenanthroline)

Andrei V. Palii,[*,†] Sergei M. Ostrovsky,[*,†] Sophia I. Klokishner,[†,‡]
Boris S. Tsukerblat,[§] Curtis P. Berlinguette,[‖] Kim R. Dunbar,[‖] and
José Ramón Galán-Mascarós[⊥]

Contribution from the Institute of Applied Physics, Academy of Sciences of Moldova, Academy Str. 5, MD 2028 Kishinev, Moldova, State University of Moldova, Mateevich Str. 60, MD 2009 Kishinev, Moldova, Chemistry Department, Ben-Gurion University of the Negev, Beer-Sheva 84105, Israel, Department of Chemistry, Texas A&M University, College Station, Texas 77842-3012, and Instituto de Ciencia Molecular, Universidad de Valencia, Dr. Moliner, 50. 46100, Burjasot, Spain

Received June 1, 2004; E-mail: Andrew.Palii@uv.es; sm_ostrovsky@yahoo.com

Abstract: We report a new theoretical model that accounts for the unusual magnetic properties of the cyanide cluster $\{[Mn^{II}(tmphen)_2]_3[Mn^{III}(CN)_6]_2\}$ (tmphen = 3,4,7,8-tetramethyl-1,10-phenanthroline). The model takes into account (1) the spin−orbit interaction, (2) the trigonal component of the crystal field acting on the ground-state cubic $^3T_1(t_2^4)$ terms of the apical Mn(III) ions, and (3) the isotropic contribution to the exchange interaction between Mn(III) and Mn(II) ions. The ground state of the cluster was shown to be the state with the total angular momentum projection $|M_J| = 15/2$; the energies of the low-lying levels obtained from this treatment increase with decreasing $|M_J|$ values, a situation that leads to a barrier for the reversal of magnetization ($U_{\rm eff} \approx 30$ cm^{-1}). The new model explains the recently discovered single-molecule magnet behavior of the $\{[Mn^{II}(tmphen)_2]_3[Mn^{III}(CN)_6]_2\}$ in contrast to the traditional approach that takes into account only the ground-state spin (S) and a negative zero-field splitting parameter ($D_S < 0$).

1. Introduction

Molecules that exhibit magnetic bistability, commonly referred to as single-molecule magnets (SMM), are of high interest due to their unusual physical properties and potential importance for high-density data storage and quantum computing.[1,2] These systems show an extremely slow relaxation of the magnetization and quantum tunneling effects at low temperatures. The existence of the phenomenon of single-molecule magnetism was first realized at the beginning of the 1990s (see review paper[1] and references therein) in the family of clusters of general formula $[Mn_{12}O_{12}(O_2CR)_{16}(H_2O)_4]$ (Mn12-ac).[3−8] Since this discovery, the study of single-molecule magnetism has become an active field, with numerous magnetic clusters exhibiting SMM properties being reported in the recent literature.[9−12] The complexity of most of these systems has precluded an analytical approach to the theory, however, and thus only phenomenological models have been applied. These models are based on the spin Hamiltonian approach dealing with the symmetry-adopted polynomials of spin operators and parameters that are left undetermined in the spin Hamiltonian. A more profound approach is required if we are to fully understand the different origins of these phenomena and develop more rational approaches to new single-molecule magnets with desired properties.

To date, nearly all of the molecules firmly established as displaying SMM behavior contain oxide bridges that mediate the magnetic exchange coupling between metal centers. A notable feature of the structures of the known oxo-bridged

---

[†] Academy of Sciences of Moldova.

[‡] State University of Moldova.

[§] Ben-Gurion University of the Negev.

[‖] Texas A&M University.

[⊥] Universidad de Valencia.

(1) Gatteschi, D.; Sessoli, R. *Angew. Chem., Int. Ed.* **2003**, *42*, 268−297.

(2) Christou, G.; Gatteschi, D.; Hendrickson, D. N.; Sessoli, R. *MRS Bull.* **2000**, *25*, 66−71.

(3) Awschalom, D. D.; Di Vencenzo, D. P. *Phys. Today* **1995**, 43−48.

(4) Sessoli, R.; Tsai, H.-L.; Schake, A. R.; Wang, S.; Vincent, J. B.; Folting, K.; Gatteschi, D.; Christou, G.; Hendrickson, D. N. *J. Am. Chem. Soc.* **1993**, *115*, 1804−1816.

(5) Sessoli, R.; Gatteschi, D.; Caneschi, A.; Novak, M. A. *Nature* **1993**, *365*, 141−143.

(6) Eppley, H. J.; Tsai, H.-L.; de Vries, N.; Folting, K.; Christou, G.; Hendrickson, D. N. *J. Am. Chem. Soc.* **1995**, *117*, 301−317.

(7) Aubin, S. M. J.; Sun, Z.; Pardi, L.; Krzystek, J.; Folting, K.; Brunel, L.-C.; Rheingold, A. L.; Christou, G.; Hendrickson, D. N. *Inorg. Chem.* **1999**, *38*, 5329−5340.

(8) Soler, M.; Chandra, S. K.; Ruiz, D.; Davidson, E. R.; Hendrickson, D. N.; Christou, G. *Chem. Commun.* **2000**, 2417−2418.

(9) Aubin, S. M. J.; Wemple, M. W.; Adams, D. M.; Tsai, H.-L.; Christou, G; Hendrickson, D. N. *J. Am. Chem. Soc.* **1996**, *118*, 7746−7754.

(10) Barra, A. L.; De Brunner, P.; Gatteschi, D.; Schultz, C. E.; Sessoli, R. *Europhys. Lett.* **1996**, *35*, 133−138.

(11) Castro, S. L.; Sun, Z.; Grant, C. M.; Bollinger, J. C.; Hendrickson, D. N.; Christou, G. *J. Am. Chem. Soc.* **1998**, *120*, 2365−2375.

(12) Andres, H.; Basler, R.; Güdel, H.-U.; Aromi, G.; Christou, G.; Büttner, H.; Ruffle, B. *J. Am. Chem. Soc.* **2000**, *122*, 12469−12477.

10.1021/ja046771a CCC: $27.50

SMMs is the low-symmetry ligand surroundings of the constituent metal ions, the result of which is a quenching of orbital angular momenta. Such molecules possess a large total spin ground state (S) arising from the isotropic Heisenberg-type magnetic superexchange, which, when combined with a negative axial zero-field splitting ($D_S < 0$), leads to the appearance of an energy barrier for spin reversal.

In the interest of producing clusters with larger spin reversal barriers, considerable attention is being focused on developing cyanide-bridged cluster systems, for which the degree of magnetic anisotropy can be more readily controlled by deliberate introduction of specific metal ions. For example, by replacing $\mathrm{Cr^{III}}$ with $\mathrm{Mo^{III}}$ in trigonal prismatic clusters of the type $[(\mathrm{Me_3tacn})_6\mathrm{MnCr_6(CN)_{18}}]^{2+}$ ($\mathrm{Me_3tacn}$ = N,N',N''-trimethyl-1,4,7-triazacyclononane; cyclam = 1,4,8,11-tetraazacyclotetradecane), the SMM molecule $[(\mathrm{Me_3tacn})_6\mathrm{MnMo_6(CN)_{18}}]^{2+}$ was obtained.[13] This cluster represents a first well-documented example of a cyano-bridged SMM. Almost simultaneously, the trigonal bipyramidal cyano-bridged cluster $[\mathrm{Mn^{III}(CN)_6}]_2[\mathrm{Mn^{II}(tmphen)_2}]_3$ (tmphen = 3,4,7,8-tetramethyl-1,10-phenanthroline) was synthesized and characterized.[14] The system hereafter abbreviated as "$\mathrm{Mn_5}$-cyanide" contains three equatorial Mn(II) and two apical Mn(III) ions. The experimental temperature dependence of the dc susceptibility indicates antiferromagnetic coupling between the Mn(II) and Mn(III) ions, and the ac-susceptibility data exhibit an out-of-phase signal that is indicative of SMM behavior.[14]

In striving to understand the magnetic properties of $[\mathrm{Mn^{III}(CN)_6}]_2[\mathrm{Mn^{II}(tmphen)_2}]_3$, we first note that the structure of the cluster contains Mn(III) ions in nearly perfect octahedral sites. As a result, the strong cubic crystal field produced by the six carbon atoms of the cyanide ligand leads to the ground spin and orbital triplet ${}^3T_1(t_2^4)$ of the Mn(III) ion. The ground state of the Mn(II) ion in the octahedral nitrogen environment is the orbital singlet ${}^6A_1(t_2^3e^2)$. In the context of the discussion of the magnetic anisotropy, it should be noted that the ${}^3T_1(t_2^4)$ state of the Mn(III) ion involves first-order orbital magnetism. This observation led us to conclude that the system under consideration must be treated differently from spin systems consisting of orbitally nondegenerate ions (mainly oxide-bridged clusters) possessing weak (second-order) single-ion anisotropy described by the zero-field splitting Hamiltonian $D_S[S_Z^2 - (1/3)S(S+1)]$ (hereunder the sign of the uniaxial D parameter corresponds to this Hamiltonian). Unlike for these molecules, one must deal with a significant local (single-ion) anisotropy arising from two unquenched orbital angular momenta of Mn(III) in $\mathrm{Mn_5}$–cyanide. This anisotropy cannot be described by the term $D_S[S_Z^2 - (1/3)S(S+1)]$. The highly anisotropic Mn(III) ions are expected to play a crucial role in the formation of a barrier for the reversal of magnetization and hence in the SMM behavior of the $\mathrm{Mn_5}$–cyanide cluster. Since the contribution of the high-spin Mn(II) ions to the global anisotropy is negligible,[15] the role of these ions is merely to increase the total angular momentum of the cluster through coupling with the Mn(III) ions via superexchange mediated by the cyanide bridges.

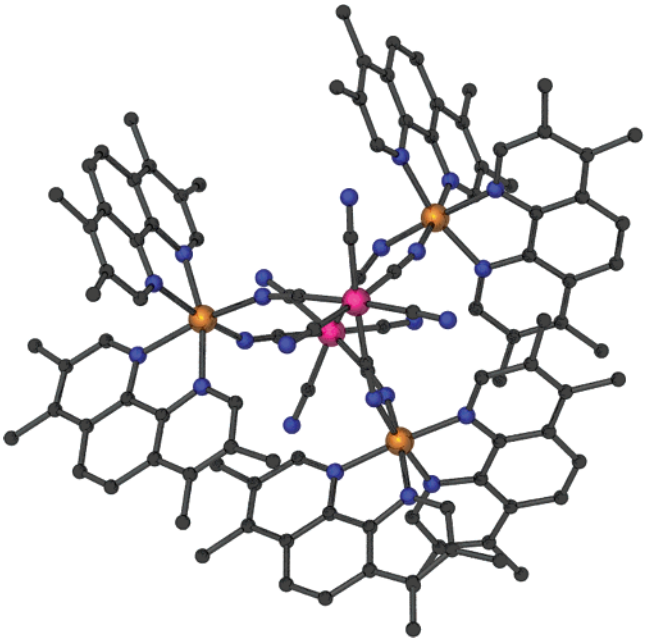

Figure 1. Molecular structure of $\{[\mathrm{Mn^{II}(tmphen)_2}]_3[\mathrm{Mn^{III}(CN)_6}]_2\}$. Mn(III): pink, Mn(II): orange, N: blue. Hydrogen atoms have been omitted for the sake of clarity.

According to the aforementioned discussion, $\mathrm{Mn_5}$–cyanide can be regarded as the first representative of a new class of SMMs based on cyanide clusters containing metal ions with unquenched orbital angular momenta. Therefore, one can expect a significant difference between the physical mechanism of the SMM behavior of the $\mathrm{Mn_5}$–cyanide and the conventional mechanism (large S in combination with negative uniaxial D_S parameter), which is relevant to the oxide-bridged spin systems. Clearly, the conventional model based on the spin Hamiltonian involving exchange interaction and a zero-field splitting term fails for this new class of SMMs, and the elaboration of a new model is required. One of the questions to be answered is how the local first-order anisotropy manifests itself in the global anisotropy of the $\mathrm{Mn_5}$–cyanide cluster. In this article, we endeavor to develop the model able to explain the magnetic properties of the $\mathrm{Mn_5}$–cyanide and its magnetic anisotropy responsible for the SMM behavior. This model takes into account the first-order single-ion anisotropy associated with the Mn(III) ions and includes the antiferromagnetic superexchange (mediated by the cyanide bridges) between Mn(III) and Mn(II) ions.

2. Model

The molecular geometry of $\mathrm{Mn_5}$–cyanide is represented in Figure 1. Each Mn(III) ion forms three linear cyanide bridges to the Mn(II) centers and is capped by three terminal cyanide ligands. The five Mn ions form a trigonal bipyramid in which two Mn(III) ions surrounded by six carbon atoms occupy the apical positions and three Mn(II) ions coordinated by the nitrogen atoms reside in the equatorial plane.[14] Due to a strong cubic crystal field produced by carbon atoms, the ground term of the Mn(III) ion in the cubic field is expected to be the low-spin ($s = 1$) orbital triplet ${}^3T_1(t_2^4)$. On the contrary, the weak crystal field induced by the nitrogen atoms gives rise to a high-spin ($s = 5/2$) ground term ${}^6A_1(t_2^3e^2)$ of each Mn(II) ion. The presence of the methylated phenanthroline ligands prevents the

---

(13) Sokol, J. J.; Hee, A. G.; Long, J. R. *J. Am. Chem. Soc.* **2002**, *124*, 7656–7657.

(14) Berlinguette, C. P.; Vaughn, D.; Cañada-Vilalta, C.; Galán-Mascarós, J.-R.; Dunbar, K. R. *Angew. Chem., Int. Ed.* **2003**, *42*, 1523–1526.

(15) Altshuler, S. A.; Kozyrev, B. M. *Electronic Paramagnetic Resonance*; Nauka: Moscow, 1972.

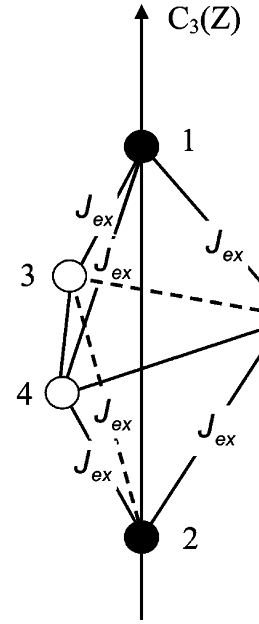

Figure 2. Metal skeleton of the Mn_5−cyanide cluster: 1, 2: Mn(III); 3, 4, 5: Mn(II).

clusters from packing with close intermolecular metal−metal distances (the closest intermolecular Mn···Mn distance is 8.77 Å). These ligands do not result in $\pi-\pi$ stacking that could extend the exchange interaction for a long distance. We will, therefore, neglect intercluster interactions and consider this to be a single-cluster problem. The adopted labeling scheme of the Mn ions is shown in Figure 2, where the numbers 1 and 2 are assigned to two Mn(III) ions and the three Mn(II) ions are labeled by 3, 4, and 5.

The following intra-ion and inter-ion interactions will be included in the model:

(i) The spin−orbit (SO) coupling operating within the ground cubic ${}^3T_1(t_2^4)$ term of each Mn(III) ion. The orbital triplet T_1 can be regarded as the state with the fictitious orbital angular momentum $l = 1$,[16,17] so that the SO coupling splits the ${}^3T_1$ term into three levels corresponding to $j = 0$ (A_1), $j = 1$ (T_1), and $j = 2$ (E,T_2), with j being the quantum number of the fictitious total angular momentum of the Mn(III) ion in the ground state.

(ii) Trigonal crystal field. Inspecting the structure of the Mn_5−cyanide cluster (Figure 1), one can conclude that the site symmetry of the Mn(III) ions is C_{3v}. The trigonal component of the crystal field splits the ground ${}^3T_1(l = 1)$ term into the orbital singlet ${}^3A_2$ ($m_l = 0$) and the orbital doublet ${}^3E(m_l = \pm 1)$. The trigonal crystal field is expected to be significantly smaller than the cubic one and will be taken into account within the first-order approximation along with the SO coupling. This expectation is in compliance with the molecular geometry of the Mn_5−cyanide cluster.

(iii) Magnetic exchange. We assume that only the superexchange interaction between Mn(II) and Mn(III) ions through the cyanide bridges affects the magnetic properties. The through-space interactions between Mn(II) ions are expected to be negligible due to the large intermetallic distances. The typical values of the parameters of exchange coupling between cyanide-bridged metal ions are of the order of several wavenumbers,[18] that is, they are 2 orders of magnitude smaller than the parameters of the SO coupling and the trigonal crystal field.

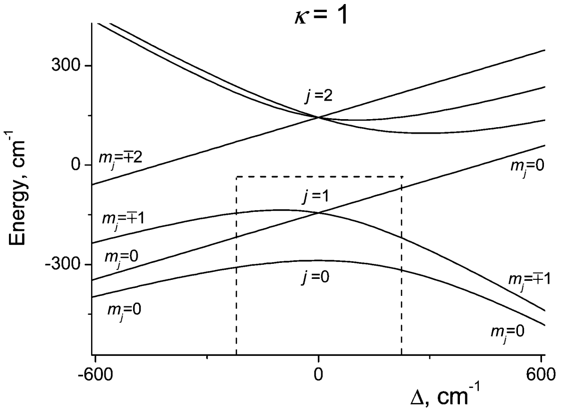

Figure 3. Splitting of the ground ${}^3T_1$ term of the Mn(III) ion by the SO coupling ($\lambda = -180$ cm^{-1}, $\kappa = 1$) and trigonal field.

The combined action of the SO coupling and the trigonal field can be described by the following single-ion Hamiltonian acting within the ${}^3T_1$ manifold of each Mn(III) ion ($i = 1,2$):

$$\boldsymbol{H}_i = -\kappa\lambda \boldsymbol{s}_i \boldsymbol{l}_i + \Delta({l_{iZ}}^2 - 2/3) \tag{1}$$

In eq 1, λ is the many-electron SO coupling parameter for ${}^3T_1(t_2^4)$ term and κ is the orbital reduction factor. The trigonal field parameter Δ is defined as the splitting of the ${}^3T_1(t_2^4)$ term. The one-electron SO coupling parameter for a free Mn(III) ion is equal to $\zeta = 360$ cm^{-1},[17] and thus the corresponding many-electron parameter for the low-spin ${}^3T_1$ state can be estimated as $\lambda = -(\zeta/2S) \approx -180$ cm^{-1}. The sign "minus" in the term $-\kappa\lambda \boldsymbol{s}_i\boldsymbol{l}_i$ appears because the matrices of the operator of the orbital angular momentum defined in T_1 and P bases differ in sign.[16]

The energy levels $E_j(|m_j|)$ of a trigonally distorted Mn(III) complex are enumerated by the absolute value of the total angular momentum projection $|m_j|$, thus reflecting the axial magnetic symmetry of the system. They are given by:

$$E_0(0) = \frac{1}{6}(-\Delta + 3\kappa\lambda - 3\sqrt{(\Delta + \kappa\lambda)^2 + 8\kappa^2\lambda^2})$$

$$E_2(0) = \frac{1}{6}(-\Delta + 3\kappa\lambda + 3\sqrt{(\Delta + \kappa\lambda)^2 + 8\kappa^2\lambda^2})$$

$$E_1(0) = \frac{1}{3}(\Delta + 3\kappa\lambda)$$

$$E_1(1) = \frac{1}{6}(-\Delta - 3\sqrt{\Delta^2 + 4\kappa^2\lambda^2})$$
$$E_2(1) = \frac{1}{6}(-\Delta + 3\sqrt{\Delta^2 + 4\kappa^2\lambda^2})$$

$$E_2(2) = \frac{1}{3}(\Delta - 3\kappa\lambda) \tag{2}$$

Here the symbol j ($j = 0$, 1, and 2) indicates the origin of the level $E_j(|m_j|)$ with a given $|m_j|$. In Figure 3, the levels (eq 2) are depicted as a function of the gap Δ. In the high-symmetry case, where $\Delta/(\kappa|\lambda|) = 0$, the energy pattern consists of three levels formed by the SO interaction in a cubic field (Figure 3):

---

[16] Sugano, S; Tanabe, Y.; Kamimura, H. *Multiplets of Transition Metal Ions in Crystals*; Academic Press: London, 1970.

[17] Abragam, A.; Bleaney, B. *Electron Paramagnetic Resonance of Transition Ions*; Clarendon: Oxford, England, 1970.

[18] Weihe, H.; Güdel, H. *Comments Inorg. Chem.* **2000**, *22*, 75.

$$E(j=0)=2\kappa\lambda,\quad E(j=1)=\kappa\lambda,\quad E(j=2)=-\kappa\lambda \tag{3}$$

This limit is magnetically isotropic. As far as the problem of the magnetic anisotropy is concerned, it must be stressed that the cases of positive and negative trigonal fields are qualitatively different. Providing that $\Delta > 0$, one can see that the low-lying part of the energy pattern consists of two levels, the ground-state singlet with $m_j = 0$ (A_2), and the excited-state non-Kramers doublet with $m_j = \pm 1$ (E). The energy gap between these levels decreases with the increase of Δ. In the case of a relatively strong trigonal field, these two levels are well separated from the excited states and can be associated with the zero-field splitting of $^3A_2$. The conventionally defined single-ion zero-field splitting uniaxial parameter D for the Mn(III) ion calculated (accurate within (λ^3/Δ^2)) with the aid of eq 2 is the following:

$$D=\frac{\kappa^2\lambda^2}{\Delta}-\frac{2\kappa^3\lambda^3}{\Delta^2} \tag{4}$$

In the limit of a strong positive trigonal field, the SO splitting (and the local anisotropy) is fully suppressed, and thus the ground state is the orbital singlet $^3A_2$ which comprises $m_j = 0(m_l = 0,\ m_s = 0)$ and $m_j = \pm 1(m_l = 0,\ m_s = \pm 1)$.

The splitting of the $^3T_1$ term of the Mn(III) ion by the negative trigonal field leads to the ground orbital doublet ^3E (orbital basis $m_l = \pm 1$). In the case of a negative trigonal field, the ground-state manifold consists of four levels (Figure 3) that can be labeled (in ascending order) as: $m_j = 0(A_1)$, $m_j = 0$ (A_2), $|m_j| = 1(E)$, and $|m_j| = 2(E)$. With an increase in the parameter $|\Delta|$, the two low-lying levels with $m_j = 0$ ($E_0(0)$ and $E_1(0)$) begin to merge, and the gap δ between these levels in the case of a strong field becomes (accurate within (λ^3/Δ^2)):

$$\delta=\frac{2\kappa^2\lambda^2}{|\Delta|}+\frac{2\kappa^3\lambda^3}{\Delta^2} \tag{5}$$

In the limit of a strong negative trigonal field, the low-lying part of the energy pattern consists of three equidistant levels that can be regarded as a result of the SO splitting of the isolated trigonal ^3E term. The set of the levels includes the accidentally degenerate level A_1, A_2 ($m_j = 0(m_l = \pm 1,\ m_s = \mp 1)$) and two non-Kramers doublets E: $m_j = \pm 1(m_l = \pm 1,\ m_s = 0)$, $m_j = \pm 2(m_l = \pm 1,\ m_s = \pm 1)$ (Figure 3). The energy gap between the neighboring doublets is $\kappa|\lambda|$. This group of the energy levels can be described by the effective axial SO coupling operator $\kappa|\lambda|l_Z s_Z$ that is operative within the ^3E basis, the SO splitting being thus reduced by the trigonal field as compared to that in the cubic $^3T_1$ term.

Regarding the magnetic exchange between metal ions, strictly speaking it cannot be described by the isotropic Heisenberg−Dirac−Van Vleck (HDVV) Hamiltonian due to the presence of unquenched orbital angular momenta, and a more general consideration based on the orbitally dependent (commonly, magnetically anisotropic) Hamiltonian is required.[19−23] To make our treatment more simple and to avoid overparameterization of the theory, we will use a simplification similar to that proposed by Lines in his study of the magnetic exchange between high-spin Co(II) ions.[24,25] We will neglect the essentially anisotropic orbitally dependent terms in the exchange Hamiltonian and retain only the isotropic contributions described by the HDVV Hamiltonian. In our recent article,[26] we have carefully analyzed the Lines approach in the framework of a more general background and have shown that this is often a good approximation. Within this approximation, the exchange Hamiltonian for the pair of the exchange-coupled metal ions (i and k) is of the form:

$$\mathbf{H}_{\mathrm{ex}}(i,k)=-2J_{\mathrm{ex}}\boldsymbol{s}_i\boldsymbol{s}_k \tag{6}$$

where the exchange parameter $J_{\mathrm{ex}} = J_{\mathrm{ex}}[\mathrm{Mn(II)} - \mathrm{Mn(III)}]$ is assumed to be the same for all Mn(II)−Mn(III) pairs in accordance with the geometry of the complex. A remark should be made concerning the sign of the exchange parameter. The results of various studies[18,27,28] clearly indicate that the superexchange interaction in cyanide-bridged species is mediated by the π orbitals of the cyanide bridge. Given that the t_2 orbitals are the ones involved in the π superexchange, only these orbitals contribute to the exchange integral. In the present cluster, the Mn(III)−CN−Mn(II) angle is close to 180°; therefore, the magnetic t_2 orbitals located on Mn(III) and Mn(II) ions are nonorthogonal, which facilitates antiferromagnetic superexchange. For this reason, we will consider only negative J_{ex} values.

The full Hamiltonian of the system is as follows:

$$\begin{aligned}\mathbf{H} = {}& -\kappa\lambda(\boldsymbol{s}_1\boldsymbol{l}_1+\boldsymbol{s}_2\boldsymbol{l}_2)-2J_{\mathrm{ex}}(\boldsymbol{s}_1+\boldsymbol{s}_2)(\boldsymbol{s}_3+\boldsymbol{s}_4+\boldsymbol{s}_5) - \\ & \Delta(l_{1Z}{}^2+l_{2Z}{}^2-4/3)+\beta\boldsymbol{H}[-\kappa(\boldsymbol{l}_1+\boldsymbol{l}_2)+g_e(\boldsymbol{s}_1+\boldsymbol{s}_2)+ \\ & g(\boldsymbol{s}_3+\boldsymbol{s}_4+\boldsymbol{s}_5)]\end{aligned} \tag{7}$$

where the last term is the Zeeman interaction, which includes orbital and spin parts, β is the Bohr magneton, and $\boldsymbol{H}$ is the applied magnetic field. We will allow the g-factor for Mn(II) ions to vary, nevertheless, and according to the physical conditions, this value is assumed to be close to 2.

The wave functions are constructed using the following scheme of the angular momenta addition:

$$\begin{aligned}&\boldsymbol{s}_1+\boldsymbol{l}_1=\boldsymbol{j}_1,\quad \boldsymbol{s}_2+\boldsymbol{l}_2=\boldsymbol{j}_2,\quad \boldsymbol{j}_1+\boldsymbol{j}_2=\boldsymbol{J}_{12},\quad \boldsymbol{s}_3+\boldsymbol{s}_4= \\ &\boldsymbol{S}_{34},\quad \boldsymbol{S}_{34}+\boldsymbol{s}_5=\boldsymbol{S}_{345},\quad \boldsymbol{J}_{12}+\boldsymbol{S}_{345}=\boldsymbol{J}\end{aligned} \tag{8}$$

where $\boldsymbol{J}$ is the total angular momentum. This scheme corresponds to the following labeling of the wave functions that will be used as the basis set for the matrix representation of the Hamiltonian (eq 7):

$$|s_1l_1(j_1)s_2l_2(j_2)(J_{12})\ s_3s_4(S_{34})s_5(S_{345})JM_J\rangle \equiv |(j_1)(j_2)(J_{12})(S_{34})(S_{345})JM_J\rangle \tag{9}$$

The matrix elements of the Hamiltonian (eq 7) can be calculated with the aid of the irreducible tensor operator technique. The

---

(19) Borras-Almenar, J. J.; Clemente-Juan, J. M.; Coronado, E.; Palii, A.V.; Tsukerblat, B. S. *J. Phys. Chem. A* **1998**, *102*, 200−213.

(20) Borras-Almenar, J. J.; Clemente-Juan, J. M.; Coronado, E.; Palii, A. V.; Tsukerblat, B. S. *Phys. Lett. A* **1998**, *238*, 164−168.

(21) Borras-Almenar, J. J.; Clemente-Juan, J. M.; Coronado, E.; Palii, A. V.; Tsukerblat, B. S. *Chem. Phys.* **2001**, *274*, 2−3, 131−144, 145−163.

(22) Borras-Almenar, J. J.; Clemente-Juan, J. M.; Coronado, E.; Palii, A. V.; Tsukerblat, B. S. *Phys. J. Sol. State Chem.* **2001**, *159*, 268−280.

(23) Borras-Almenar, J. J.; Clemente-Juan, J. M.; Coronado, E.; Palii, A. V.; Tsukerblat, B. S. *J. Chem. Phys.* **2001**, *114*, 1148.

(24) Lines, M. E. *J. Chem. Phys.* **1971**, *55*, 2977.

(25) Ginsberg, A. P. *Inorg. Chim. Acta* **1971**, *5*, 45.

(26) Palii, A. V.; Tsukerblat, B. S.; Coronado, E.; Clemente-Juan, J. M.; Borras-Almenar, J. J. *J. Chem. Phys.* **2003**, *118*, 5566.

(27) Babel, D. *Comments Inorg. Chem.* **1986**, *5*, 285.

(28) Entley W. R.; Girolami, G. S. *Science* **1995**, *268*, 397.

description of this method can be found elsewhere.[29−33] For the convenience of the reader, some details of the calculations of the matrix elements of the full Hamiltonian are given as Supporting Information. Regarding the energy levels for spin clusters, a new computational procedure developed in ref 34 should be mentioned.

The full matrix of the Hamiltonian (eq 7) including the interactions between seven angular momenta (five spins and two orbital angular momenta) as well as the Zeeman interaction is rather large (the dimension of the space is 17 496). To simplify the time-consuming procedure of diagonalization, we have assumed that the energy levels of the system associated with the highest group of levels of the Mn(III) ions (three levels resulting from the $j = 2$ multiplet) do not contribute significantly to the magnetic properties of the Mn_5−cyanide cluster until room temperature for which the experimental data are available. This approximation is reasonable in the range of relatively weak trigonal fields when the separation between two excited groups of levels arising from $j = 1$ and $j = 2$ significantly exceeds the splitting caused by the magnetic exchange. Consequently, one can exclude the states with $j = 2$ from the basis, thus reducing the number of states to 3456. In Figure 3, the range of the parameter Δ suitable for this approximation and the truncated basis are conventionally indicated by the dashed box. The matrix is reduced to the tridiagonal form using the standard Householder algorithm, and the eigenvalues and eigenvectors of this tridiagonal matrix are found using QL algorithm.

3. Results and Discussion

Before proceeding to the fitting of the experimental magnetic susceptibility data, let us discuss how the trigonal crystal field and the SO interaction in the Mn(III) ion affect the energy pattern of the cluster coupled by antiferromagnetic exchange. The above analysis indicates that the sign of the local magnetic anisotropy is defined by the sign of the trigonal component of the crystal field. As a result, the sign of Δ is expected to be of crucial importance for determining the global magnetic anisotropy of the Mn_5−cyanide cluster. For this reason, we have analyzed the two cases ($\Delta > 0$ and $\Delta < 0$) separately.

Providing the presence of a relatively strong positive trigonal field, each Mn(III) behaves as a spin $s = 1$ ion with quenched (to a second order) orbital angular momentum. In such a case, the Mn_5−cyanide cluster can be considered as a spin system, and the magnetic anisotropy of the cluster can be described by the second-order zero-field splitting Hamiltonian $D(s_{1Z}^2 + s_{2Z}^2)$ with the positive single-ion constant D (eq 4). Since the Mn(II) ions are isotropic, the effective D_S value for the isolated ground-state multiplet $S = 11/2$ (under the condition of antiferromagnetic Mn(II)−Mn(III) exchange) is positive; in this case the ground level corresponds to $|M_S| = 1/2$, and the low-temperature magnetic anisotropy defined as $\Delta\chi = \chi_\perp - \chi_\parallel$ is positive. Under a more general condition of a moderate trigonal field when the gap $E_1(1) - E_1(0)$ (eq 2) and the isotropic exchange are comparable, all exchange levels are effectively mixed. In Figure 4, we show the scheme of the low-lying levels calculated for the moderate positive trigonal field ($\Delta = 250$ cm^{-1}). This energy pattern demonstrates that, in the case of a moderate field, the ground state of the system possesses the minimum projection of the total angular momentum $|M_J| = 1/2$ and that, for the low-lying levels, the quantum number $|M_J|$ increases (non-monotonically) with an increase in energy. This energy pattern corresponds to an effective positive global anisotropy of the system and thus proves to be incompatible with the experimental observation of a barrier for the reversal of magnetization, that is, SMM behavior.

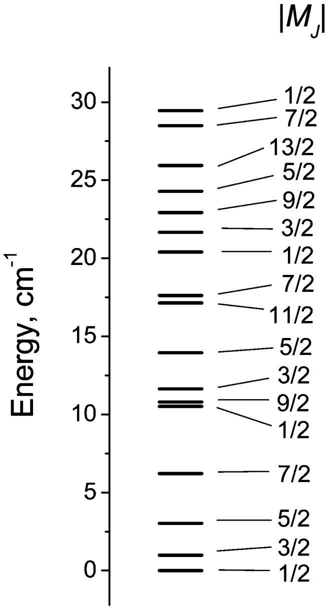

Figure 4. Energy scheme of low-lying levels in the case of positive trigonal crystal field: $J_{ex} = -3.8$ cm^{-1}, $\Delta = 250$ cm^{-1} ($\kappa = 0.8$).

In the case of a negative trigonal field, there is a qualitatively different physical picture due to the fact that the orbital doublet $^3E(m_l = \pm1)$ carries a first-order orbital contribution. It should be noted that, for a sufficiently strong trigonal field, the two low-lying singlets $E_0(0)$ and $E_1(0)$ are magnetic, although $m_j = 0$. In fact, the nonvanishing matrix elements of the Zeeman interaction, which is operative within this pair of levels, are found as:

$$\langle m_j = 0(m_l = \pm1,\, m_s = \mp1)|\beta(-\kappa \boldsymbol{l} + g_e \boldsymbol{s})\boldsymbol{H}|\, m_j = 0(m_l = \pm1,\, m_s = \mp1)\rangle = \mp(\kappa + g_e)\beta H_z \quad (10)$$

In this case, the perpendicular component of the Zeeman interaction vanishes, and the system can be referred to as fully anisotropic. From Figure 3, one can see that the magnetic contributions associated with the next levels $E_1(1)$ and $E_2(2)$ are also fully anisotropic.

As follows from eq 10, the low-temperature local magnetic anisotropy associated with the Mn(III) ion is negative ($\chi_\parallel > 0$, $\chi_\perp = 0$) if the trigonal crystal field is sufficiently strong. Calculations of the energy pattern show that, at low temperatures, the global magnetic anisotropy is also negative, which would thus lead to the necessary conditions for the formation of a barrier for the reversal of magnetization. This conclusion,

---

(29) Varshalovich, D. A.; Moskalev, A. N.; Khersonskii, V. K. *Quantum Theory of Angular Momentum*; World Scientific: Singapore, 1988.

(30) Bencini, A.; Gatteschi, D. *Electron Paramagnetic Resonance of Exchange Coupled Systems*; Springer-Verlag: Berlin, 1989.

(31) Borras-Almenar, J. J.; Clemente, J. M.; Coronado, E.; Tsukerblat, B. S. *Inorg. Chem.* **1999**, *38*, 6081.

(32) Borras-Almenar, J. J.; Clemente, J. M.; Coronado, E.; Tsukerblat, B. S. *J. Comput. Chem.* **2001**, *22*, 985.

(33) Tsukerblat, B. S.; Palii, A.V.; Mirovitskii, V. Yu.; Ostrovsky, S. M.; Turta, K.; Jovmir, T.; Shova, S.; Bartolome, J.; Evangelisti, M.; Filoti, G. *J. Chem. Phys.* **2001**, *115*, 9528−9535.

(34) Waldmann, O. *Phys. Rev. B* **2001**, *61*, 6138−6144.

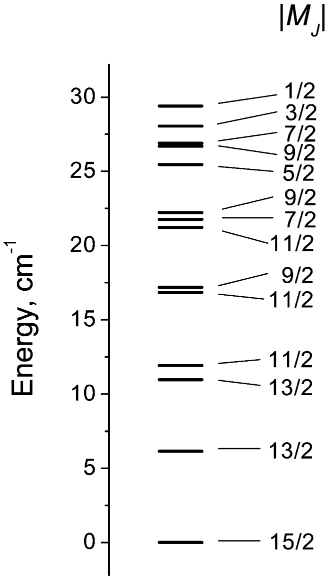

Figure 5. Energy scheme of low-lying levels in the case of negative trigonal crystal field: $J_{ex} = -3.8$ cm^{-1}, $\Delta = -251$ cm^{-1} ($\kappa = 0.8$).

which is also valid for the region of moderate trigonal field, is illustrated in Figure 5, wherein the energy pattern of the system (up to 30 cm^{-1}) is given for the following set of parameters: $J = -3.8$ cm^{-1}, $\Delta = -251$ cm^{-1}, $\kappa = 0.8$. Later it will be shown that this set of parameters fits the experimental χT vs T curve. The main features of this pattern are that the ground level possesses the projection $|M_J| = 15/2$ and that $|M_J|$ decreases with increasing energy. This means that the global anisotropy proves to be negative (irregularities in the disposition of the excited levels vs $|M_J|$ do not change this conclusion), and this result is compatible with the observed SMM behavior of Mn$_5$−cyanide. Note that the global negative anisotropy of this kind is a consequence of the unquenched orbital contribution in the case of a negative trigonal field.

It is worth noting that the scheme of the low-lying levels depicted in Figure 5 is qualitatively different from the conventional scheme of the levels obtained for an isolated S multiplet of a spin cluster. In the latter case, the levels are numbered by $|M_S|$, and the energies monotonically increase with the decrease of $|M_s|$ in accordance with the law $D_S(M_S^2 - S(S+1)/3)$ ($D_S < 0$). In the case under consideration, the energy scheme does not follow this simple rule; rather, there is a more complicated scheme of levels that involves irregularities in the disposition of the levels as a function of $|M_J|$ (Figure 5). Such a situation occurs because the states with the fixed value of $|M_J|$ belonging to different values of the total momentum J are strongly mixed by the trigonal field. Similar alternation of the levels may appear in the energy spectrum of spin systems if the mixing of different spin multiplets by the anisotropic terms of the spin Hamiltonian is taken into account. This mixing turns out to be important when the single-ion anisotropic terms are of the same order as the isotropic exchange such that the ground spin multiplet is not well separated from the excited ones.

At this point, we further inspected the magnetic properties given the presence of a negative trigonal field. Due to the trigonal symmetry, the magnetic susceptibility tensor has two principal values, $\chi_{ZZ} \equiv \chi_{\parallel}$ and $\chi_{XX} = \chi_{YY} \equiv \chi_{\perp}$, related to the C_3 axis. These values are calculated using the conventional definition:

$$\chi_{\alpha\alpha} = N_A k_B T \frac{\partial^2}{\partial H_\alpha^2}[\ln Z(H_\alpha)]_{H_\alpha \to 0} \tag{11}$$

where $\alpha = X, Y, Z$. The partition function is given by:

$$Z(H_\alpha) = \sum_i \exp[-E_i(H_\alpha)/k_B T] \tag{12}$$

where $E_i(H_\alpha)$ are the energies of the system in the presence of the magnetic field, and they are obtained numerically as the result of the diagonalization of the energy matrix corresponding to the full Hamiltonian (eq 7). Finally, the susceptibility of the powder sample is calculated with the use of the approximate formula:

$$\chi = \frac{1}{3}(\chi_{\parallel} + 2\chi_{\perp}) \tag{13}$$

Sample calculations of χT are shown in Figures 6 and 7. Hereafter, we use the above-mentioned value $\lambda = -180$ cm^{-1} for the SO coupling parameter. To reduce the number of the adjustable parameters in the fitting of the experimental data we will set $\kappa = 0.8$, which is a typical value of the orbital reduction factor of a Mn(III) ion in cyanide complexes.[17]

An increase of $|J_{ex}|$ shifts both the low-temperature maximum and the minimum of the χT curve toward the higher temperatures (Figure 6). On the contrary, the temperatures corresponding to these points are essentially insensitive to the trigonal field (Figure 7). In fact, when J_{ex} is constant, the change in the trigonal field affects mainly the low-temperature part of the χT vs T curve so that the increase of $|\Delta|$ leads to a decrease of χT in the low-temperature region. One can thus conclude that the magnetic exchange is the main interaction affecting the positions of the low-temperature maximum and minimum of χT. This finding allowed us to estimate the parameter J_{ex} at a fixed value of Δ (say, at $\Delta = 0$) and then use this value of J_{ex} as a starting point in the best fit procedure.

Figure 8 displays the temperature dependence of χT measured for crushed single crystal at 1000 G over the temperature range 1.8−300 K[14] and the theoretical curve calculated for the set of the best fit parameters. The observed room temperature χT value is ~13.70 emu·K·mol^{-1} and decreases to 10.4 emu·K·mol^{-1} as the temperature is lowered to 45 K, after which temperature χT increases to a maximum of 15.7 emu·K·mol^{-1} at 4.0 K.

The best fit is achieved for $\Delta = -251$ cm^{-1}, $J_{ex} = -3.8$ cm^{-1}, and $g = 1.95$, with the agreement criterion $(1/N)\sum[(\chi T)_{expt} - (\chi T)_{calcd}]^2/(\chi T)_{expt}{}^2$ being equal to 2.9×10^{-3} ($N = 52$ is the number of the experimental points). One can see that the theoretical curve calculated with this set of parameters is in a satisfactory agreement with the experimental data in that it reproduces the minimum at 45 K and the slope of the curve in the high temperature region. The relatively small value obtained for the trigonal crystal field parameter is favorable for the approximation adopted thus far and is also in accord with the structural data that indicate nearly perfect octahedral environments for the Mn(III) ions. The best fit value of the exchange parameter falls into the range of typical values for the superexchange parameters mediated by the cyanide bridges.[18]

Strictly speaking, the nonmonotonic disposition of the energy levels corresponding to the set of the best fit parameters (Figure 5) does not allow one to identify the height of the barrier for

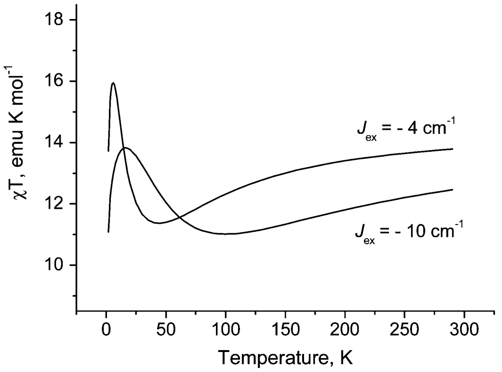

Figure 6. Influence of the magnetic exchange on χT shown for $\Delta = -250$ cm^{-1} ($\kappa = 0.8$).

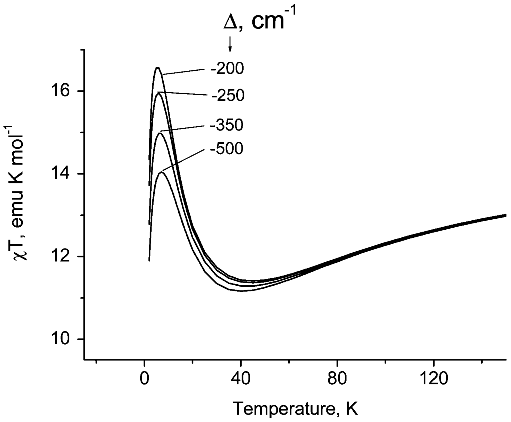

Figure 7. Influence of the trigonal crystal field on χT shown for $J_{ex} = -4$ cm^{-1} ($\kappa = 0.8$).

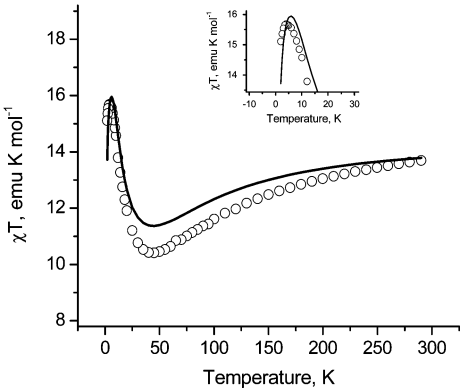

Figure 8. Temperature dependences of χT. Circles: experimental data. Solid line: theoretical curve calculated with the best fit parameters $J_{ex} = -3.8$ cm^{-1}, $\Delta = -251$ cm^{-1}, $g = 1.95$ ($\kappa = 0.8$). Inset: low-temperature part of χT vs T.

Mn$_5$−cyanide cluster according to the energy gap between the levels with the maximum (ground state) and minimum $|M_J|$ values (15/2 and 1/2). Nevertheless, since this gap is relevant to relaxation pathways it can be considered as a useful measure of the barrier. As follows from Figure 5, this effective barrier for Mn$_5$−cyanide cluster is ~30 cm^{-1}. The spin model employed in ref 14 for a preliminary discussion gives the value 10 cm^{-1} for the barrier that corresponds to $D = -0.348(3)$ cm^{-1}, but no experimental barrier value directly from ac measurements was reported since the blocking temperature is below 2 K. Probably more experimental data could be helpful for the justification of the model and more reliable estimation of the barrier. The fitting of the magnetization vs H and T is expected to give more information.

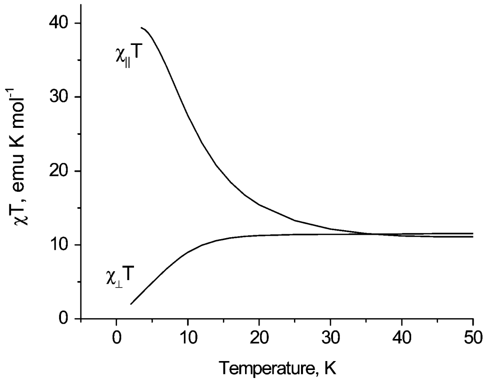

Figure 9. Temperature dependences of $\chi_{||}T$ and $\chi_{\perp}T$ calculated with the set of the best fit parameters: $J_{ex} = -3.8$ cm^{-1}, $\Delta = -251$ cm^{-1}, $g = 1.95$ ($\kappa = 0.8$).

The temperature dependence of $\chi_{||}T$ and $\chi_{\perp}T$ calculated with the set of the best fit parameters is presented in Figure 9. It can be seen that, at low temperatures, the system exhibits strong axial anisotropy with $\Delta\chi = \chi_{\perp} - \chi_{||} < 0$. This observation is illustrated by the scheme of the low-lying energy levels calculated with the set of the best fit parameters (Figure 5). The decrease of $|M_J|$ with an increase in energy accounts for the magnetic behavior of the system and, in particular, the sharp decrease of χT in the temperature range 4−45 K. At the same time, the model reveals the conditions under which the system demonstrates the observed SMM behavior for the Mn$_5$−cyanide cluster.[14]

4. Concluding Remarks

The model developed in this study represents a first attempt to reveal the underlying mechanism responsible for the SMM behavior of cyanide clusters containing highly anisotropic transition metal ions with unquenched orbital angular momenta. The model includes a trigonal crystal field and a SO interaction operating within the ground state of the Mn(III) ions and the isotropic exchange interaction between Mn(II) and Mn(III) ions. The model was shown to account for the observed dc magnetic susceptibility of the Mn$_5$−cyanide cluster. The interplay between the strong single-ion anisotropy arising from the trigonal crystal field, combined with the SO interaction and antiferromagnetic Heisenberg-type exchange, was shown to produce an appreciable barrier for the reversal of magnetization. The proposed model provides a satisfactory agreement between the observed and calculated dc magnetic susceptibilities and also confirms the ac susceptibility evidence for SMM behavior of the Mn$_5$-cyanide cluster. These findings lend insight into the conditions under which the barrier for the reversal of magnetization appears in clusters containing metal ions with unquenched orbital angular momenta. In contrast to traditional SMMs that can be treated as spin clusters, the first-order single-ion anisotropy of the Mn(III) ion was found to be responsible for the formation of the barrier. It is interesting to note, however, that exchange-biased quantum tunneling has been noted in a supramolecular dimer consisting of two SMM Mn$_4$ clusters, each of which contains three Mn(III) ions and one Mn(IV) ion.[35] The Mn(III)

---

(35) Wernsdorfer, W.; Aliaga-Alcalde, N.; Hendrickson, D.; Christou, G. *Nature* **2002**, *416*, 406−409.

ion in each cluster subunit is in a sufficiently low-symmetry crystal field such that the orbital contribution is strongly quenched. Consequently, the Mn_4 cluster behaves like a spin system.

Finally, it should be noted that the model contains several simplifying assumptions. First, we neglected the orbitally dependent terms in the exchange Hamiltonian. These terms are expected to contribute to the global magnetic anisotropy of the system, thus affecting the barrier for the reversal of magnetization. Second, a truncated basis was used in the magnetic susceptibility calculations. Also, the effects of Jahn−Teller vibronic interactions for the orbitally degenerate $^3T_1$ term of the Mn(III) ion may be also important both for the formation of the barrier and for the relaxation processes. These considerations remain as open issues and will be considered in future developments of these types of models.

Acknowledgment. The research described in this publication was made possible in part by Award No. MOC2-2611-CH-04 of the U.S. Civilian Research & Development Foundation for the Independent States of the Former Soviet Union (CRDF) and Award No. MTFP-04-07 of the Moldovan Research and Development Association (MRDA) under funding from the CRDF.

Supporting Information Available: Application of the irreducible tensor operator technique to the evaluation of the matrix elements of the Hamiltonian (eq 7). This material is available free of charge via the Internet at http://pubs.acs.org.

JA046771A